



HAL
open science

Surface texturing to reduce temperature in mechanical seals

Kacou Dingui, Noël Brunetière, Jean Bouyer, Mohand Adjemout

► **To cite this version:**

Kacou Dingui, Noël Brunetière, Jean Bouyer, Mohand Adjemout. Surface texturing to reduce temperature in mechanical seals. Tribology Online, 2020, 15 (4), pp.222-229. 10.2474/trol.15.222 . hal-03039807

HAL Id: hal-03039807

<https://hal.science/hal-03039807>

Submitted on 4 Dec 2020

HAL is a multi-disciplinary open access archive for the deposit and dissemination of scientific research documents, whether they are published or not. The documents may come from teaching and research institutions in France or abroad, or from public or private research centers.

L'archive ouverte pluridisciplinaire **HAL**, est destinée au dépôt et à la diffusion de documents scientifiques de niveau recherche, publiés ou non, émanant des établissements d'enseignement et de recherche français ou étrangers, des laboratoires publics ou privés.



Distributed under a Creative Commons Attribution - NonCommercial - NoDerivatives 4.0 International License

Surface texturing to reduce temperature in mechanical seals

Kacou Dingui^{1,2}, Noël Brunetière ¹, Jean Bouyer ¹ and Mohand Adjemout ³

1) Institut Pprime, CNRS-Université de Poitiers-ISAE ENSMA

SP2MI, Bât. H1, 11 boulevard marie et Pierre Curie, TSA 41123, 86073 Poitiers Cedex 9, France

2) ENS Paris Saclay

61 Avenue du Président Wilson, 94230 Cachan, France

3) Groupe Latty

1 Rue Xavier Latty, 28160 Brou, France

*Corresponding author: noel.brunetiere@univ-poitiers.fr

Based on the paper presented and published at the BHR Group 25th International Conference on Fluid Sealing, 4-5 March 2020, Manchester

Mechanical seals are composed of two annular flat rings in contact and relative motion to ensure sealing of a rotating shaft. Because of friction in the sealing interface, a significant temperature rise can be experienced in the contact. Two decades ago, it has been shown that creating a network of shallow dimples on one sealing surface can help to create a lubricant film in the interface and thus reduce friction. Since then, many research works have been carried out on the so-called surface texturing, showing the interest of surface modification for mechanical seals.

In the present work, several surface patterns, defined by numerical simulations and machined by plasma etching on stainless steel rings were tested. The rings were mounted on a test bench in which they slide against a sapphire disk counter face. This disk is transparent to infrared radiation and allows interface temperature measurements by infrared thermography. It is shown that all the tested surface texture patterns exhibit a temperature rise at least 2 times lower than with flat smooth surfaces. A slight difference between the different dimple shapes is obtained indicating that the temperature and friction are more controlled by texture area and surface roughness rather than by the texture pattern.

Keywords: mechanical seal, surface texture, friction, temperature, infrared thermography

1. Introduction.

Mechanical seals are composed of two annular flat rings in contact and relative motion to ensure sealing of rotating shafts. The flat geometry of the seal faces is not favorable to the generation of a fluid film by hydrodynamic lubrication [1-3]. In order to reduce wear and friction, it could be interesting to develop features to help in the lubrication of the faces. More than fifty years ago, Anno et al. [4] showed that creating micro-pillars on one of the seal faces promotes fluid film generation. Two years later [5], they showed that micro-dimples are also efficient while maintaining a low leakage level. In this pioneering work, photo-etching was used to create the surface pattern, which make the industrial application difficult. Three decades later, thanks to the development of laser technology, Etsion et al. [6] used laser surface texturing (LST) to create dimples and confirmed the results of Anno et al [5]. LST appears to be a very convenient method for surface modification [7] allowing the application of surface texture to many lubricated components including journal bearings, piston rings and seals [8, 9].

Even if many texture manufacturing techniques are now available [10], the spherical cap or cylindrical dimples are probably the most used type of surface texture in experimental studies [11-16]. These types of surface texture exhibit significant friction reduction. However, the theory is not able to demonstrate the positive effect of surface texture. Numerical simulations based on the Reynolds equation coupled with a mass-conserving cavitation algorithm show that spherical or cylindrical dimples are inefficient for hydrodynamic load generation [17,18] because the amount of load generated is very small compared to the load that must be bear by the seal [18]. These dimples work as single isolated bearings without any collective effect between the cavities [19]. In fact, it was shown that the hydrodynamic load generation observed in experiments is due to the interaction between dimples and surface roughness [18] and that dimples cannot generate a sufficient load on their own. Using other texture shapes (square, pyramidal or triangular shapes) with different orientation can slightly improve their performance [19,20]. It was show by Adjemout et al. [19] that a great improvement can be achieved if a collective effect between the dimples is generated. The most effective solution they found is composed of triangular dimples placed base to base. They showed that thanks to this texture, it is possible to reduce friction and contact temperature by 50% [21].

In the present paper, the experimental work started in paper [21] is continued with different shapes of surface texture. The idea is to compare the optimal triangular dimples to usual dimples shapes (square dimples, cylindrical cavities, other triangle configuration) which are less efficient according to the lubrication theory. The operating temperatures in the sealing interface with the different surface texture patterns are measured by infrared thermography and compared to find

out which one is the best solution.

2. Material and methods.

2.1. Seals and surface texture.

The mechanical seal used in this work is an unbalanced seal with a rotating ring made of stainless steel. This ring is textured by ion-etching technique through a mask, carburized and coated with Diamond Like Carbon (DLC) (figure 1). More details on the surface texturing technique can be found in reference [22]. The main characteristics of the seal are given in table 1. Four texture patterns (presented in figure 1) have been tested as well as a smooth surface. The geometrical parameters of the texture patterns are based on numerical simulations results [19,21]. These surfaces were measured with a white light interferometer TalySurf CCI 6000. An example of surface measurement is presented in figure 2 and the main parameters of the surfaces are presented in table 2. The groove size is its diameter or its width depending on the geometry of the texture. The surface roughness indicated in table 2 was measured on the top surface out of the dimples. It can be noted that the grooves are very shallow (less than one micron) but at least two times the roughness height S_q . The groove depth and size are based on values used in numerical studies [19, 21] but show a slight deviation due to manufacturing uncertainty [22].

Due to the polishing process a slight curvature of the seal ring surface can be seen in the central part of the sealing area (figure 2). Examples of radial surface profiles measured on the five different surfaces are presented in figure 3. A polynomial fit (thick line) is added to highlight the curvature of each profile. The radius of curvature of the surface varies from 0.44 to 0.93 m leading to submicron height variations of the same order of magnitude as the roughness height and texture depth.

2.2. Test rig

A cross section of the test cell is presented in figure 4. Two identical mechanical seals are installed back to back in the test cell to ensure an axial force balance. The seals are fed by water at 0.5 MPa and 40°C by an hydraulic equipment. An electrical motor is used to rotate the seals at speeds varying from 500 to 3000 rpm. The operating conditions are summarized in table 3. The stators of the two seals have been replaced by sapphire disks to allow visualization of the seal interface. Several thermocouples are used to measure the fluid temperature, the ambient temperature and sapphire surface temperature. The leakage of the seals is collected by two drains and measured by a weighting system. To ensure an accurate leakage measurement, several drops of fluid need to be collected. During the tests of about 10 minutes per

operating condition, the leakage levels were too small (leakage volume varying between zero or one drop of water) to ensure a reliable measurement. The parameter is thus not presented in the results section.

The sapphire has a lower thermal conductivity than the silicon carbide generally used for the seal seat material (35 W.m⁻¹.K⁻¹ compared to 150 W.m⁻¹.K⁻¹) and higher temperature levels are expected in the sealing interface. However, the sapphire has values of the thermal expansion coefficient and the elastic modulus very close to that of the silicon carbide, leading to small face deformations compared to the seal counter-face [21] as it the case with silicon carbide. It is thus expected that results obtained with the sapphire disk, even if higher in terms of temperature, are similar to what would be obtained in a real seal composed of a silicon carbide face.

2.3. Infrared thermography

An infrared camera FLIR SC7000 is placed in front of the test cell to capture the radiative flux emitted by the seal rings (figures 4 and 5). Since the sapphire disk is not fully transparent and the seal rings are reflective, the radiative flux captured by the camera is composed of an ambient emission, the disk emission and the seal ring emission (figure 6). The total radiative flux thus depends on the seal rings emissivity, sapphire disk transmissivity and refraction indices. The seal face temperature is finally obtained using the camera calibration curve. The seal face temperature is calculated on a radial band (blue rectangle in figure 5) after averaging in the circumferential direction, giving thus a radial temperature profile. Since the water film between the faces is very thin (a micron or less in thickness), it is assumed, as in paper [21], that it is fully transparent and at the same temperature as the seal faces. The water film is therefore not taken into account in the balance of radiative fluxes. The full calibration and calculation processes are described in the following section.

According to Reungoat and Tournerie, the total radiative flux, I_{cam} , recorded by the camera in the configuration of figure 6 is:

$$I_{cam} = \left(R_1^- + \frac{T_1^2 \rho_3}{1 - \rho_3 R_1^+} \right) I_{amb} + \left(E_1^- + \frac{E_1^+ T_1 \rho_3}{1 - \rho_3 R_1^+} \right) I_1 + \frac{\varepsilon_3 T_1}{1 - \rho_3 R_1^+} I_3 \quad (1)$$

Where I_{amb} , I_1 and I_3 are respectively the black body radiation emitted by the environment, the sapphire disk and the seal face, respectively. The coefficients with index 1 are related to the sapphire disk and index 3 to the seal face. Because of the Kirchoff law, the following relations exist between the coefficients [23]:

$$\varepsilon_3 + \rho_3 = 1 \quad (2)$$

$$R_1^- + E_1^- + T_1 = 1 \quad (3)$$

$$R_1^+ + E_1^+ + T_1 = 1 \quad (4)$$

The coefficients can be expressed as:

$$T_1 = \frac{(1-\rho_{air/1})(1-\rho_{1/2})\tau_1}{1-\rho_{air/1}\rho_{1/2}\tau_1} \quad (5)$$

$$R_1^- = \frac{\rho_{air/1} + \tau_1^2 \rho_{1/2} (1-2\rho_{air/1})}{1-\rho_{air/1}\rho_{1/2}\tau_1} \quad (6)$$

$$R_1^+ = \frac{\rho_{1/2} + \tau_1^2 \rho_{air/1} (1-2\rho_{1/2})}{1-\rho_{air/1}\rho_{1/2}\tau_1} \quad (7)$$

The reflection coefficients at media interfaces can be calculated from the refraction indices of the media [23]:

$$\rho_{air/1} = \frac{(n_{air}-n_1)^2}{(n_{air}+n_1)^2} \quad (8)$$

$$\rho_{1/2} = \frac{(n_1-n_2)^2}{(n_1+n_2)^2} \quad (9)$$

The refraction indices of the media can be found in the literature and are given in table 4. The only missing coefficients are the emissivity of the rotor ε_3 and the transmissivity of the sapphire disk τ_j .

2.3.1 Camera calibration

The first step consists in the camera calibration. The camera is placed in front of a black body. Since there is no reflection, the camera records the radiative flux I_0 emitted by the black body. By varying the temperature T of the black body, it is possible to obtain the calibration curve of the camera:

$$I_{cam} = I_0(T) \quad (10)$$

2.3.2 Seal face emissivity

The rotational seal ring is placed on a monitored heating system. The radiative scheme of figure 6 is simplified since media 1 and 2 are removed. The radiative equation is thus:

$$I_{cam} = (1 - \varepsilon_3)I_{amb} + \varepsilon_3 I_3 = (1 - \varepsilon_3)I_0(T_{amb}) + \varepsilon_3 I_0(T_3) \quad (11)$$

Knowing the calibration curve of the camera, the ambient temperature T_{amb} and the rotor temperature T_3 , it is possible to calculate the emissivity ε_3 of the rotor. The value of this coefficient is presented in figure 7 as a function of the surface temperature.

2.3.3 Sapphire transmissivity

To determine the transmissivity of the sapphire disk, it is placed between the camera and a black body. Referring to figure 6, it is equivalent to replace medium 2 by air and solid 3 by a black body with an emissivity equal to 1. Equation

(1) is strongly simplified in this case:

$$I_{cam} = R_1^- I_{amb} + E_1^- I_1 + T_1 I_3 = R_1^- I_0(T_{amb}) + E_1^- I_0(T_1) + T_1 I_0(T_3) \quad (12)$$

Knowing the calibration curve of the camera, the ambient temperature T_{amb} , the sapphire temperature T_1 and the black body temperature T_3 , it is possible to calculate the transmissivity τ_1 of the sapphire disk. The value of this coefficient is presented in figure 8 as a function of the black body temperature.

2.3.4 Temperature calculation

Knowing the calibration curve of the camera and the radiative coefficients of the media, it is possible to calculate the rotor temperature by solving equation (13):

$$I_{cam} = \left(R_1^- + \frac{T_1^2 \rho_3}{1 - \rho_3 R_1^+} \right) I_0(T_{amb}) + \left(E_1^- + \frac{E_1^+ T_1 \rho_3}{1 - \rho_3 R_1^+} \right) I_0(T_1) + \frac{\varepsilon_3 T_1}{1 - \rho_3 R_1^+} I_0(T_3) \quad (13)$$

A thermocouple is used to measure T_{amb} and a second one is stuck on the external surface of the sapphire disk to measure its external surface temperature T_1^{ext} . To solve the problem, it is assumed that the average sapphire temperature is the average of the rotor temperature and its external temperature:

$$T_1 \approx 0.5(T_1^{ext} + T_3) \quad (14)$$

It is then possible to solve equation (13). This equation being non-linear because of the dependence of the coefficients to the temperature and because of the calibration curve, the Newton method is used to obtain the rotor surface temperature.

3. Results

Each test was performed three times to ensure repeatability of the measurements. The results presented are an average of the results of the three tests.

Figure 9 presents radial temperature profiles obtained with the five different surface textures at rotational speeds of 1500, 2500 and 3000 rpm. The profiles are the average of the three tests carried out and the error bars indicate the minimum and maximum temperature values recorded during the three experiments. Generally speaking, whatever is the surface, the temperature at the interface increases with the rotating speed, as expected. Moreover, the temperature is lower at outer radius where the sealed fluid, which ensures cooling of the seal faces, is located. For most of the surfaces, the highest temperature is observed at the outlet side of the sealing interface. This is due to the slight curvature appearing during polishing (see figures 2 and 3) providing lowest film thickness close to the middle of the sealing interface (see ref [21]). The smooth and triangle 2 samples are the same as those tested in reference [21]. It can be seen that very close

temperature values are found, showing the repeatability of the tests. For the four textured surfaces (figure 9 a – d), it can be seen that the seal face temperature is significantly reduced compared to the smooth surfaces (figure 9 e). This shows the beneficial effect of texture to reduce friction in the contact.

To make the comparison easier, the average temperature rise in the contact for each surface is presented as a function of speed in figure 10. The benefit of using surface texture can be clearly seen. At 3000 rpm, the surface temperature rise can be divided by 2 to 3 depending on the surface patterns used.

The reduction in sealing interface temperature is generally explained by an increase in fluid film thickness due to the hydrodynamic pressure generated by the dimples. During the tests, the seal leakage was collected. However, it was not possible to measure any leakage for all the samples due to the sensitivity limit of the measuring method. It means that, even if the film thickness is increased, the leakage remains small enough so that it evaporates before reaching the weighting system used for leakage measurement. The effect of film thickness changes and temperature variations on the seal leakage are so small that they cannot be measured during the tests.

4. Discussion

These results first show that even very shallow grooves (submicron depth between 0.22 and 0.31 μm , see table 2) can significantly improve the behavior of a mechanical seal as shown in recent papers [19, 21]. However, it was shown in several papers [17-19] that usual dimples such as spherical caps, cylindrical dimples, square shaped texture are not efficient because they cannot provide sufficient lift-off to completely balance the load applied to the seal. This is due to the fact that each dimple works as a single bearing and without any collective effect. The effective friction reduction that is, however, experimentally observed [5-9, 11-16] is, according to numerical simulation, due to the interaction of surface roughness with the dimples [18].

The surface texture composed of triangular dimples placed base to base was proposed in paper [19] to create a collective effect between the dimples and provide sufficient lift-off to reach full hydrodynamic regime. These textures (triangle 1 and triangle 2 in figure 1 and table 2) were expected to give better results due to better texture arrangements. The present experimental results show that it is not the case. It is probably due to the fact that the interaction with roughness has a stronger effect than the texture shape itself. Indeed, in papers [19, 21] it was shown that the film thickness

obtained with triangular dimples is a fraction of microns, close to the surface roughness standard deviation Sq measured on the samples of this study (see table 2).

Even if all the dimple types provide at least 50% of temperature decrease compared to smooth surfaces, some of them lead to lower operating temperature. Knowing the average size of the dimples, it is possible to calculate the local area density a (the ratio of the dimple area over the unit cell area) and the total area density A calculated using the full sealing interface (table 4). There is a difference between the two values because the surfaces are not fully textured, depending on the texture type (see figure 1). Additional parameters such as the surface curvature R , the aspect ratio and the roughness to depth ratio are also reported in table 5. The average temperature rise measured at the highest speed is also given in table 5.

For each geometrical parameter presented in table 5 a correlation coefficient with the temperature rise has been calculated and presented in figure 11.

Based on this analysis, it appears that the total area density A of the texture is the most significant influencing parameter. An increase of the texture area leads to a decrease in temperature. In previous research works on textured seals [12-15], the dependence of friction and temperature on texture area density A is not monotonous as in the current work. It is probably due to the fact that a much larger interval was explored compared to the present work and that deeper grooves were used. An important parameter is also the roughness height Sq . The higher the roughness, the lower the temperature. This conclusion is in line with the findings of paper [18] showing that the performance is reached thanks to an interaction between the roughness and the texture. It is confirmed by the strong influence of the ratio of the roughness height Sq to the groove depth h_g . Finally, the groove size or related parameters have limited effect on the surface temperature. The surface curvature R also has a limited effect on the results, as indicated by its low correlation with the temperature rise. Its effect will be ignored in the next part.

A simple explanation of the effect of the texture area ratio A can be proposed. If it assumed that the film thickness out of the dimples is h_0 and that the dimple depth is h_g , the power P dissipated by viscous friction can be expressed as follows:

$$P = \mu V^2 S \left(\frac{1-A}{h_0} + \frac{A}{h_0+h_g} \right) = \mu V^2 \frac{S}{h_0} \left(1 - A \frac{h_g}{h_0+h_g} \right) \quad (15)$$

where μ is the fluid viscosity, V the sliding speed and S the sealing area. The dissipated power is a linear decreasing

function of A . If it is assumed the heat convection coefficients vary in a limited range and that the heat conduction coefficients of the materials are constant, the temperature rise is approximately proportional to the dissipated power and thus a linear decreasing function of the texture area ratio A . The measured average temperature rise at 3000 rpm is presented as a function of the total area density in figure 12 for each surface texture. The smooth surface result has also been included in the figure showing that the linear relationship extends to total texture area density when A equals zero.

However, this linear relation can only be obtained if the film thickness, the groove depth and the fluid viscosity do not vary significantly from one case to the other. If the viscosity variations are limited to less than 4% based on the temperature measurements, the groove depth changes of about 30% between the different seal rings (table 2) and it is not possible to estimate the variation of h_0 . Moreover the surface curvature and the thermal deformation will affect the fluid film geometry [19]. A numerical analysis would be necessary to get a better understanding of the experimental results and a better identification of the mechanisms providing the friction and temperature reduction. More particularly, the interaction of surface roughness with surface texture can be analyzed as well as real seal materials.

5. Conclusion

This paper presents an experimental study of textured mechanical face seal. The seal faces temperature is measured by infrared thermography through a transparent sapphire disk used as the stator of the seals. Different texture shapes were used with a depth varying from 0.22 to 0.31 μm and a total area ratio covered by grooves in the range 0.18-0.25. These very shallow grooves allow to decrease the temperature of the sealing interface of at least 50%. The performance appears to be independent of the texture shape but related to the total area density and the surface roughness height. These experimental findings confirm the numerical results from [18] showing that interaction of roughness and surface texture is a key parameter in the behavior of textured mechanical face seal.

6. Acknowledgments

This work was supported by the ANR under the reference ANR-11-RMNP-0008 and by the French government program "Investissements d'Avenir" (LABEX INTERACTIFS, reference ANR-11-LABX-0017-01).

This work was partially presented and published at the BHR Group 25th International Conference on Fluid Sealing, 4-5 March 2020, Manchester. BHR Group is thank for allowing the authors to publish this work in Tribology Online.

7. References

- [1] Lebeck, A., "Parallel Sliding Load Support In the Mixed Friction Regime. Part 1 - The Experimental Data," *Journal of Tribology*, 109, 1987, 189-195.
- [2] Lebeck, A., "Parallel Sliding Load Support In the Mixed Friction Regime. Part 2 - Evaluations of the Mechanisms," *Journal of Tribology*, 109, 1987, 196-205.
- [3] Brunetière, N., Francisco, A., "Lubrication Mechanisms Between Parallel Rough Surfaces," *Tribology Letters*, 67, 2019, 116
- [4] Anno, J.; Walowit, J., Allen, C., "Microasperity Lubrication," *Proc. 3rd International Conference on Fluid Sealing*, Cambridge, England, April 1967, 9-20.
- [5] Anno, J.; Walowit, J., Allen, C., "Load Support and Leakage from Microasperity-Lubricated Face Seals," *Proc. 4th International Conference on Fluid Sealing*, Philadelphia, USA, May 1969, 199-204.
- [6] Etsion, I.; Halperin, G., Greenberg, Y., "Increasing Mechanical Seals Life with Laser-Textured Seal Faces," *Proc. 15th International Conference on Fluid Sealing*, Maastricht, Netherlands, 1997, 3-11.
- [7] Etsion, I., "State of the Art in Laser Surface Texturing," *Journal of Tribology*, 127, 2005, 248-253.
- [8] Gropper, D.; Wang, L., Harvey, T. J., "Hydrodynamic lubrication of textured surfaces: A review of modeling techniques and key findings," *Tribology International*, 94, 2016, 509 – 529.
- [9] Rosenkranz, A.; Grützmacher, P. G.; Gachot, C., Costa, H. L., "Surface Texturing in Machine Elements – A Critical Discussion for Rolling and Sliding Contacts," *Advanced Engineering Materials*, 21, 8, 2019, 1900194.
- [10] Coblas, D.; Fatu, A.; Maoui, A., Hajjam, M., "Manufacturing textured surfaces: State of art and recent developments," *Journal of Engineering Tribology*, 229, 2015, 3-29.
- [11] Yu, X.; He, S., Cai, R., "Frictional Characteristics of Mechanical Seals with a Laser-textured Seal Face," *Journal of Materials Processing Technology*, 129, 2002, 463-466.
- [12] Wang, X.; Kato, K., Adachi, K., "The Lubrication Effect of Micro-Pits on Parallel Sliding Faces of SiC in Water," *Tribology Transactions*, 45, 2002, 294-301.
- [13] Wang, X., Kato, K., "Improving the Anti-Seizure Ability of SiC Seal in Water with RIE Texturing," *Tribology Letters*, 14, 2003, 275-280.
- [14] Wan, Y., Xiong, D.-S., "The effect of laser surface texturing on frictional performance of face seal," *Journal of Materials Processing Technology*, 197, 2008, 96 – 100.

- [15] Yan, D.; Qu, N.; Li, H., Wang, X., “Significance of Dimple Parameters on the Friction of Sliding Surfaces Investigated by Orthogonal Experiments,” *Tribology Transactions*, 53, 2010, 703-712.
- [16] Wang, T.; Huang, W.; Liu, X.; Li, Y., Wang, Y., “Experimental Study of Two-phase Mechanical Face Seals with Laser Surface Texturing,” *Tribology International*, 72, 2014, 90-97.
- [17] Qui, Y., Khonsari, M., “On the Prediction of Cavitation in Dimples Using a Mass-Conservative Algorithm,” *Journal of Tribology*, 131, 2009, 041702.
- [18] Brunetière, N., Tournerie, B., “Numerical Analysis of a Surface-Textured Mechanical Seal Operating in Mixed Lubrication Regime,” *Tribology International*, 49, 2012, 80-89.
- [19] Adjemout, M.; Brunetiere, N., Bouyer, J., “Numerical analysis of the texture effect on the hydrodynamic performance of a mechanical seal,” *Surf. Topo.: Metr. and Prop.*, 4, 2016, 014002.
- [20] Meng, X.; Bai, S., Peng, X., “Lubrication film flow control by oriented dimples for liquid lubricated mechanical seals,” *Tribology International*, 77, 2014, 132 – 141.
- [21] Adjemout, M.; Brunetière, N., Bouyer, J., “Friction and temperature reduction in a mechanical face seal by a surface texturing: comparison between TEHD simulations and experiments,” *Tribology Transactions*, 61, 2018, 1084-1093.
- [22] Adjemout, M.; Andrieux, A.; Bouyer, J.; Brunetière, N.; Marcos, G., Czerwicz, T., “Influence of the real dimple shape on the performance of a textured mechanical seal,” *Tribology International*, 115 , 2017, 409 – 416.
- [23] Reungoat, D., Tournerie, B., “Temperature Measurement by Infrared Thermography in a Lubricated Contact: Radiometric Analysis,” *Proceedings of the Eurotherm Seminar 42: Quantitative InfraRed Thermography*, Editions Europeennes Thermique et Industrie, 1994.

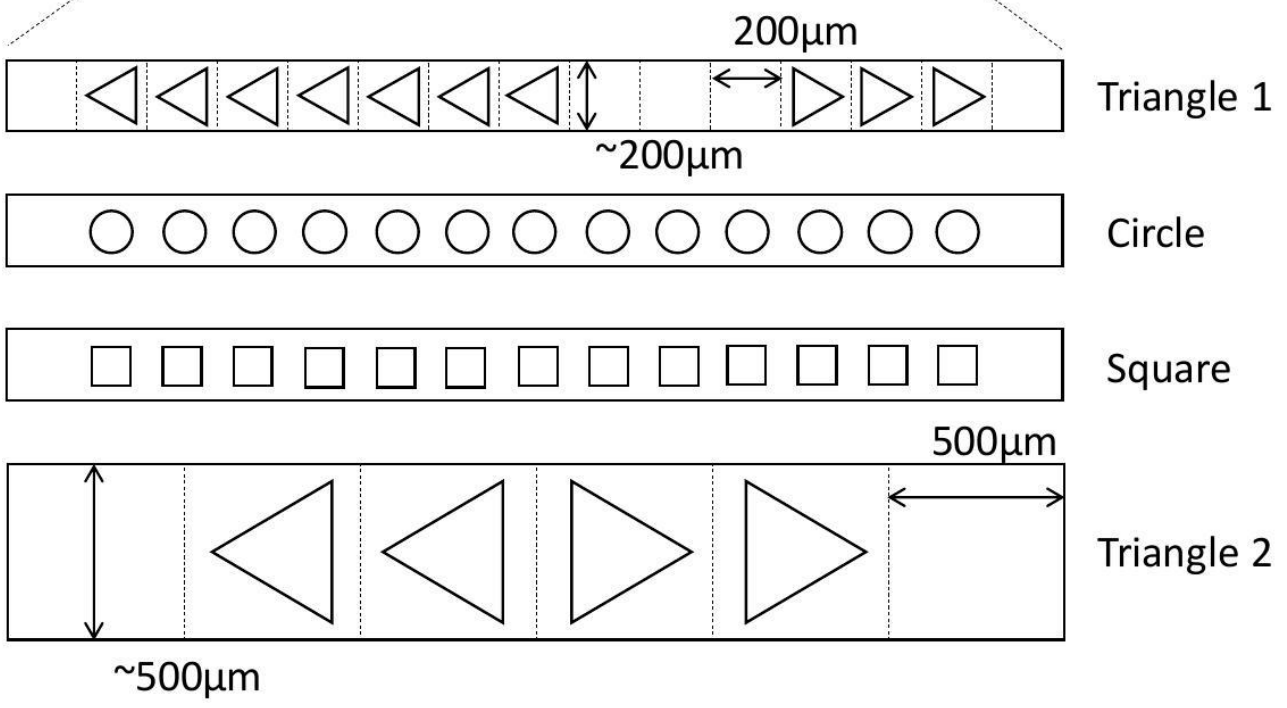
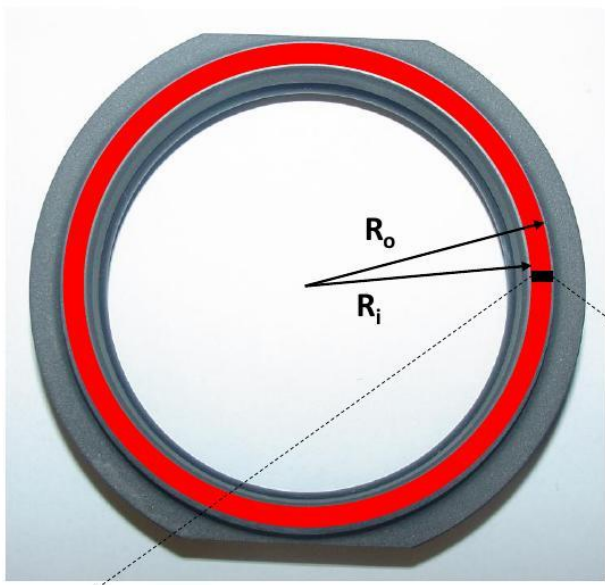


Fig. 1 Textured seal ring

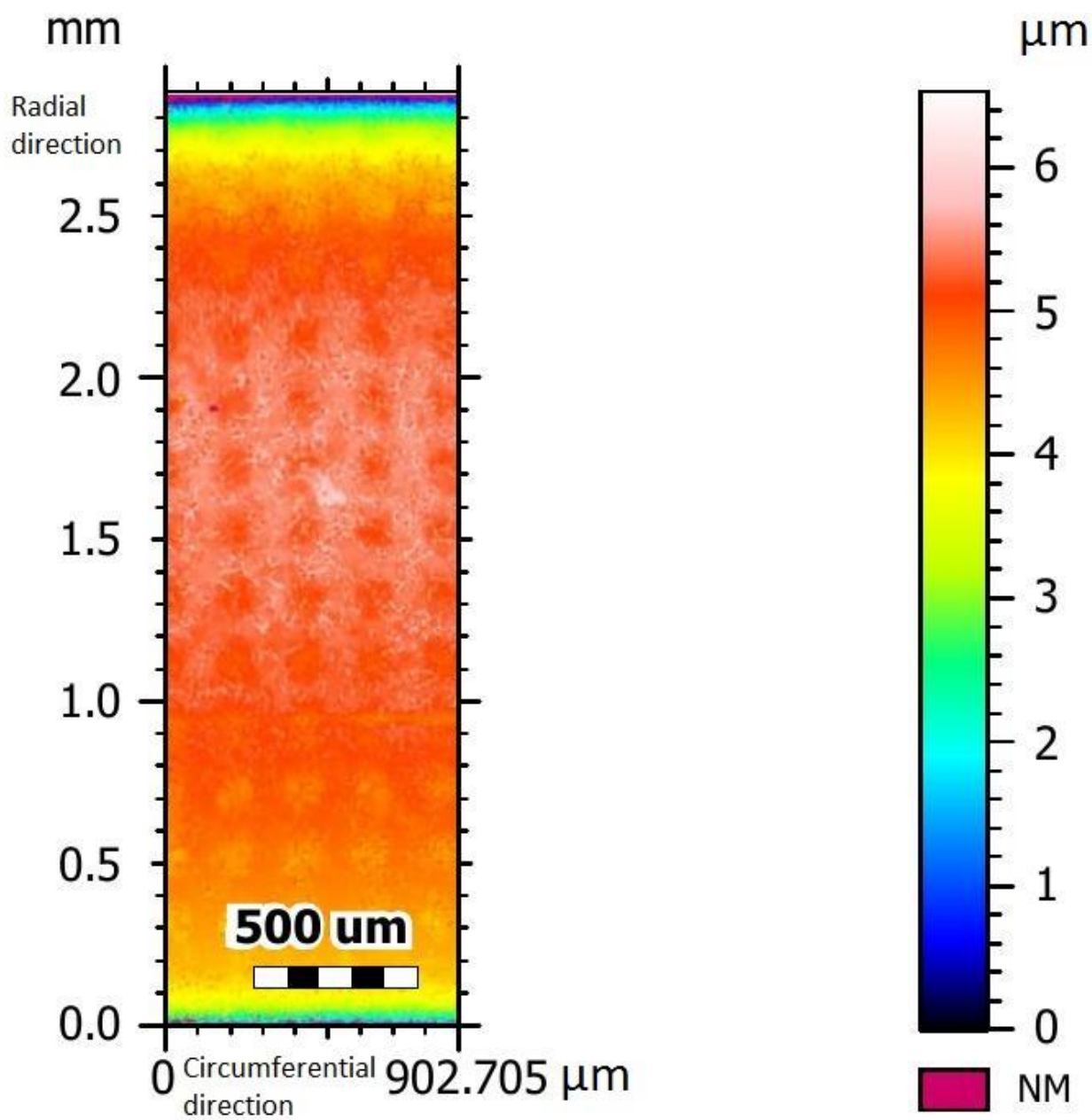


Fig. 2 Topography of one seal face with circular dimples (NM: non-measured point).

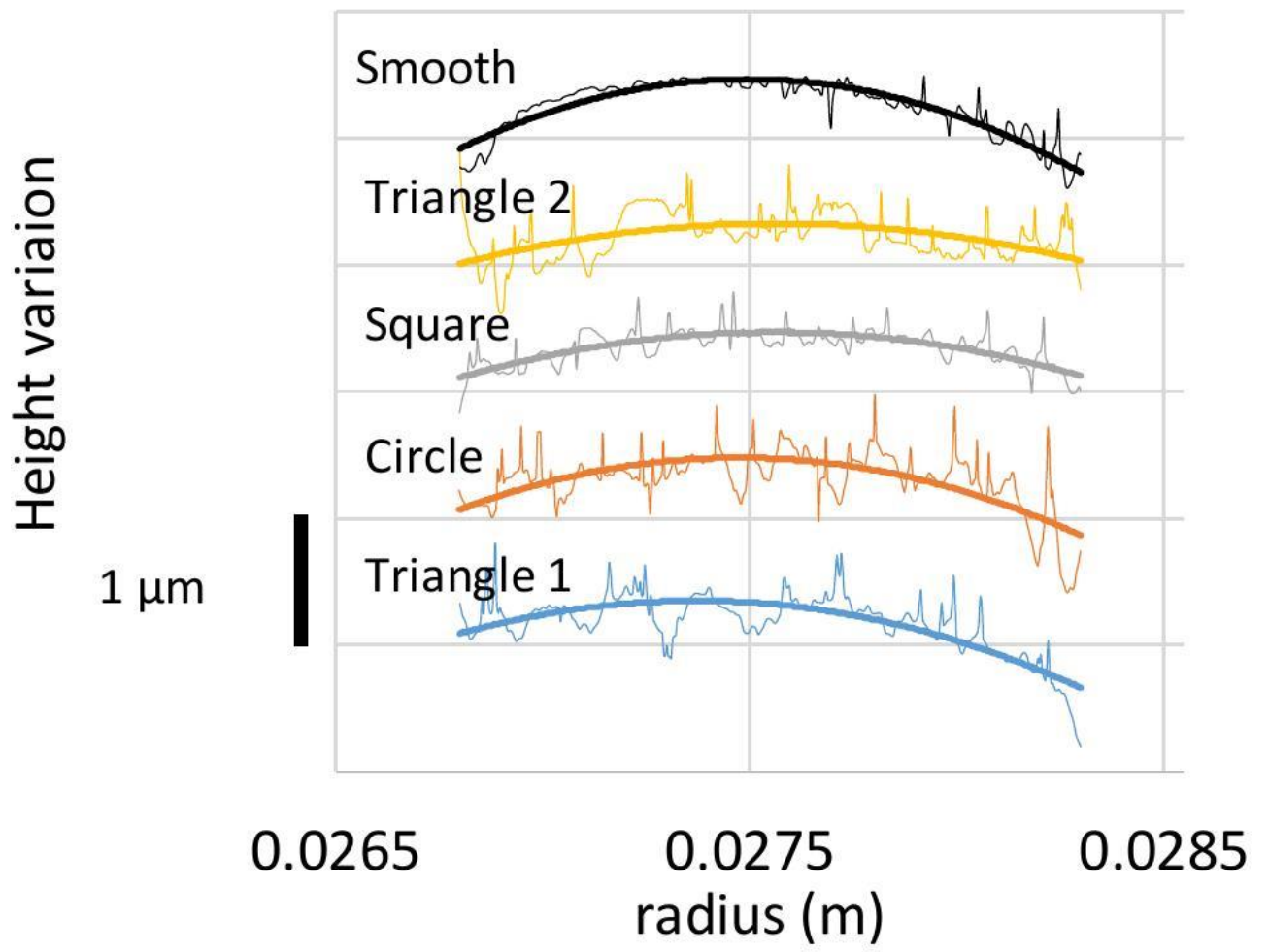


Fig. 3 Examples of radial profiles of the surfaces with a polynomial fit (thick line)

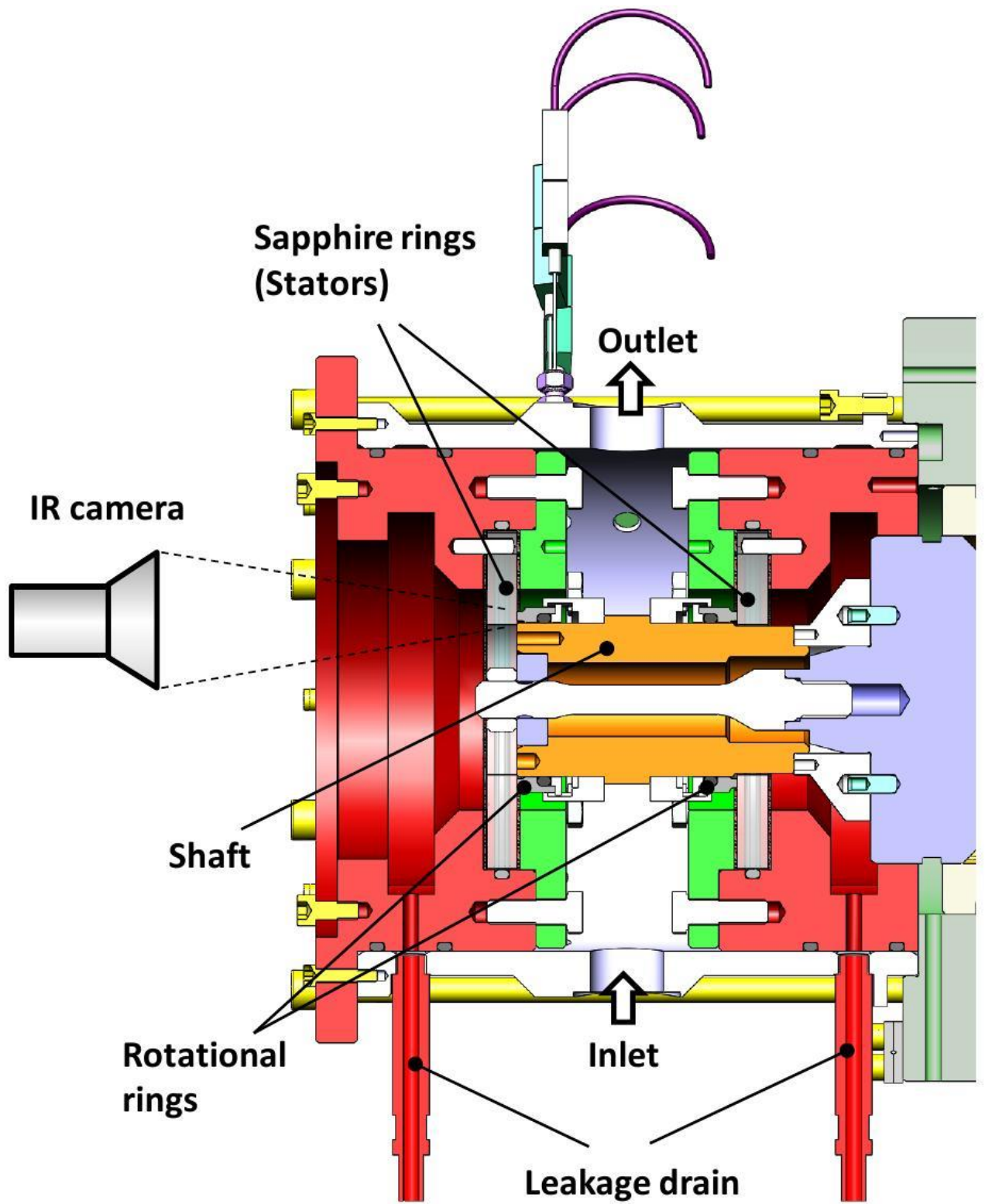


Fig. 4 Experimental cell

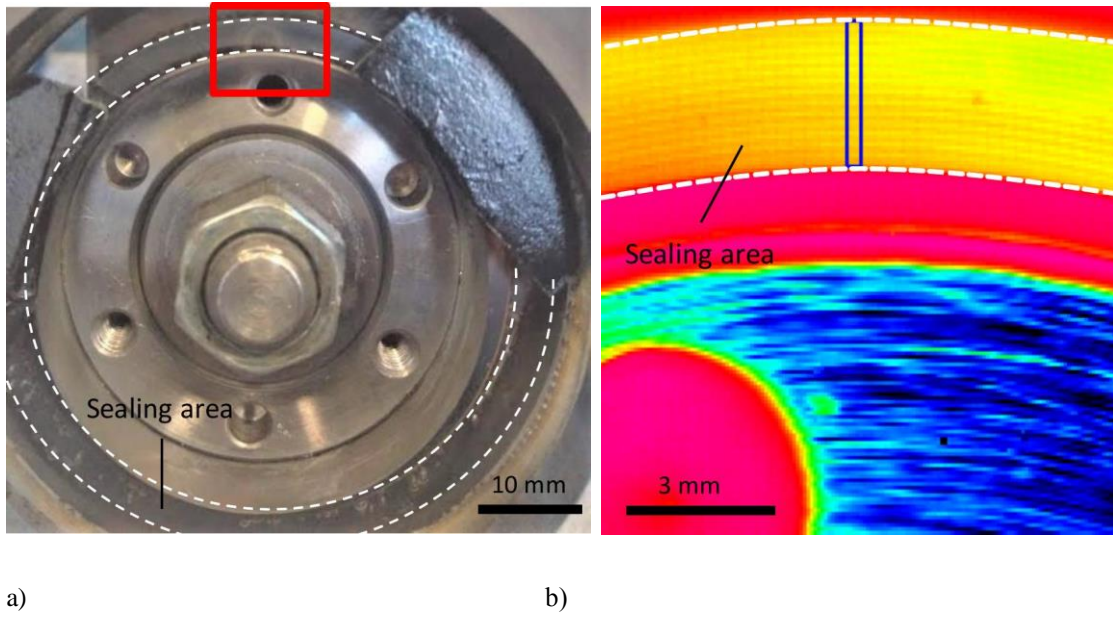


Fig. 5 a) View of the front of the test cell – b) Infrared view within the red square. The blue rectangle corresponds to the area analyzed to calculate the temperature.

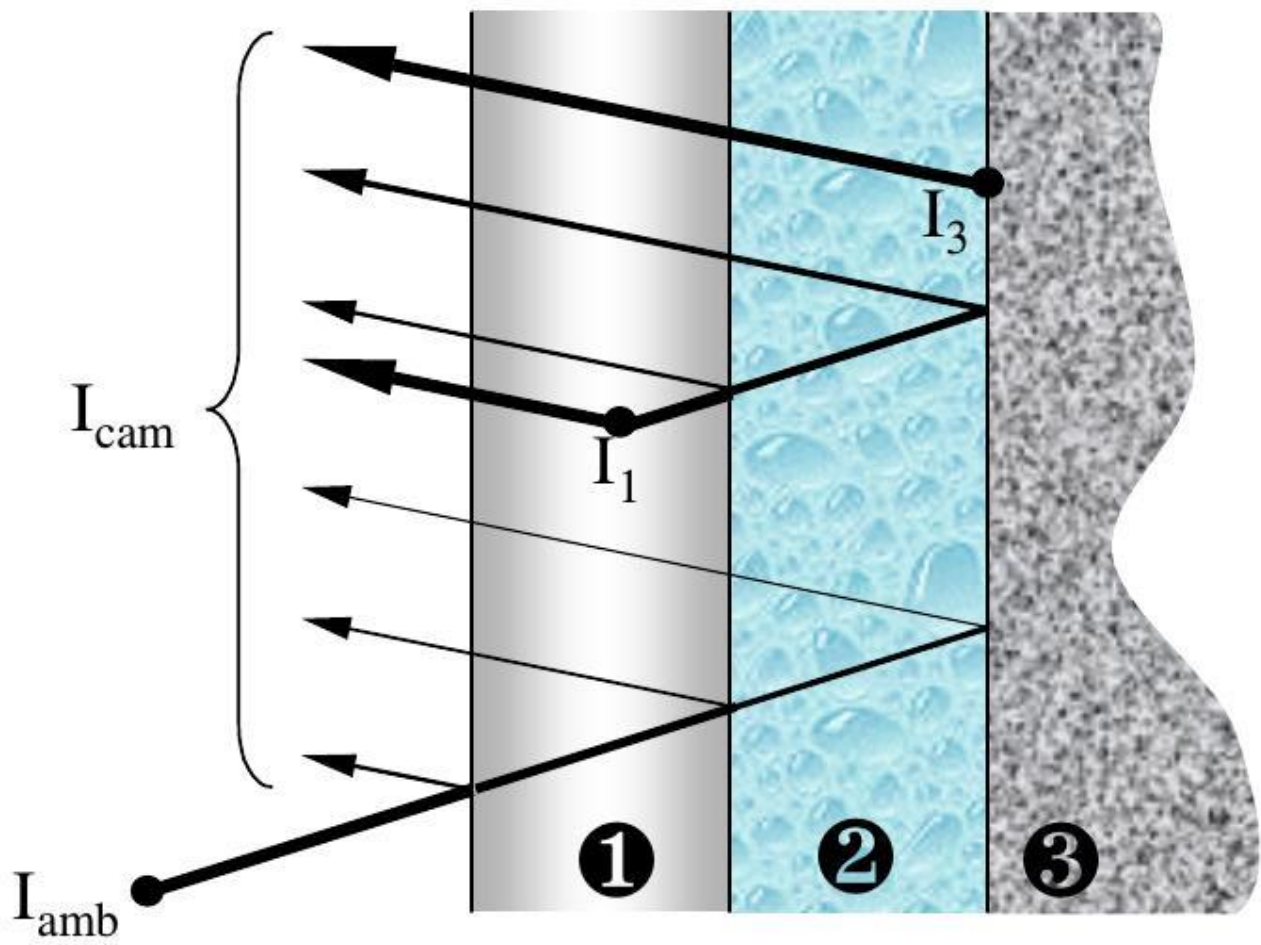


Fig. 6 Radiative scheme of the problem: Test condition: 1 = sapphire disk, 2 = water film, 3 = rotational ring –
 Transmissivity calibration: 1 = sapphire disk, 2 = air, 3 = black body.

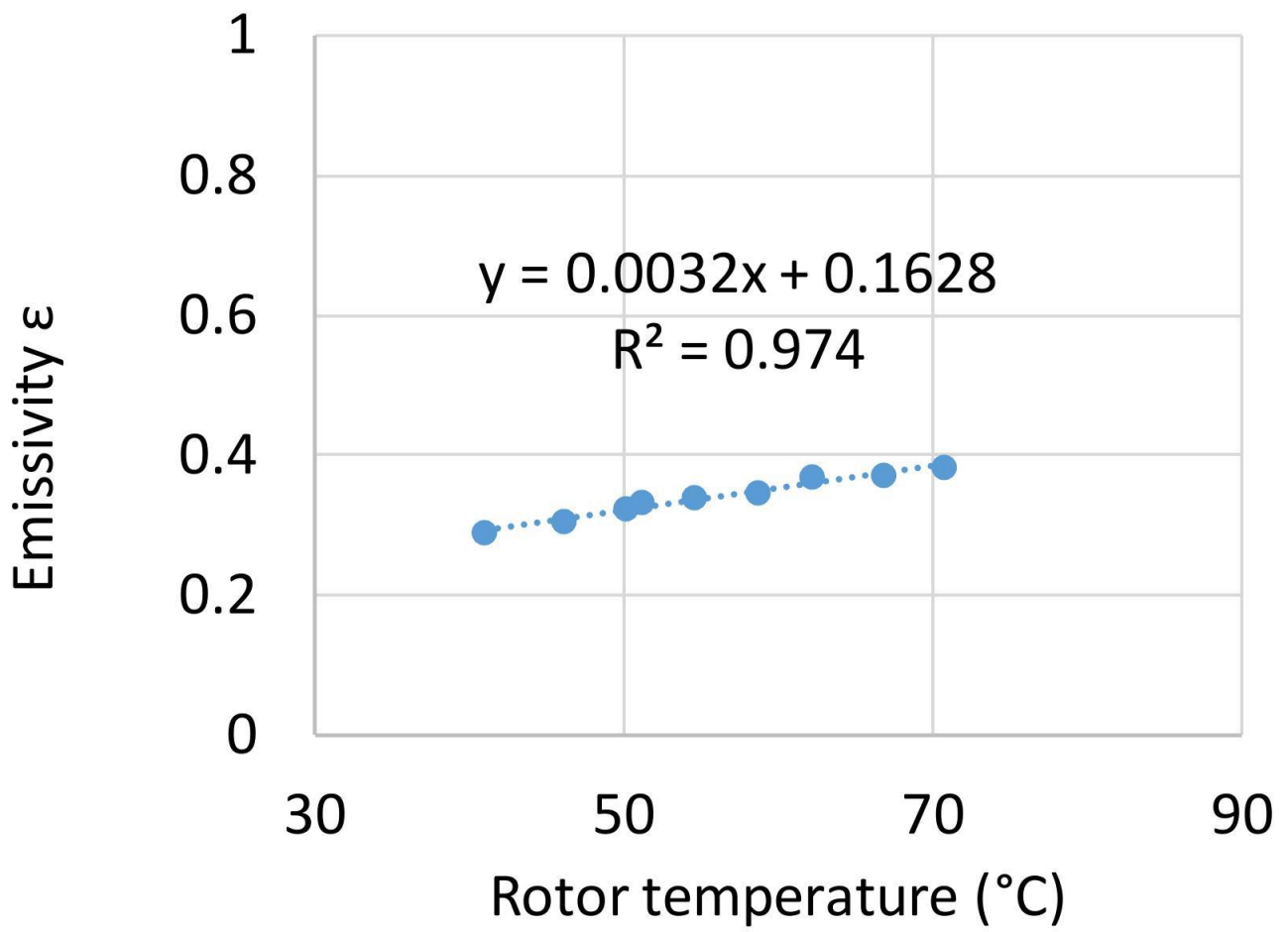


Fig. 7 Emissivity of the rotor as a function of its temperature

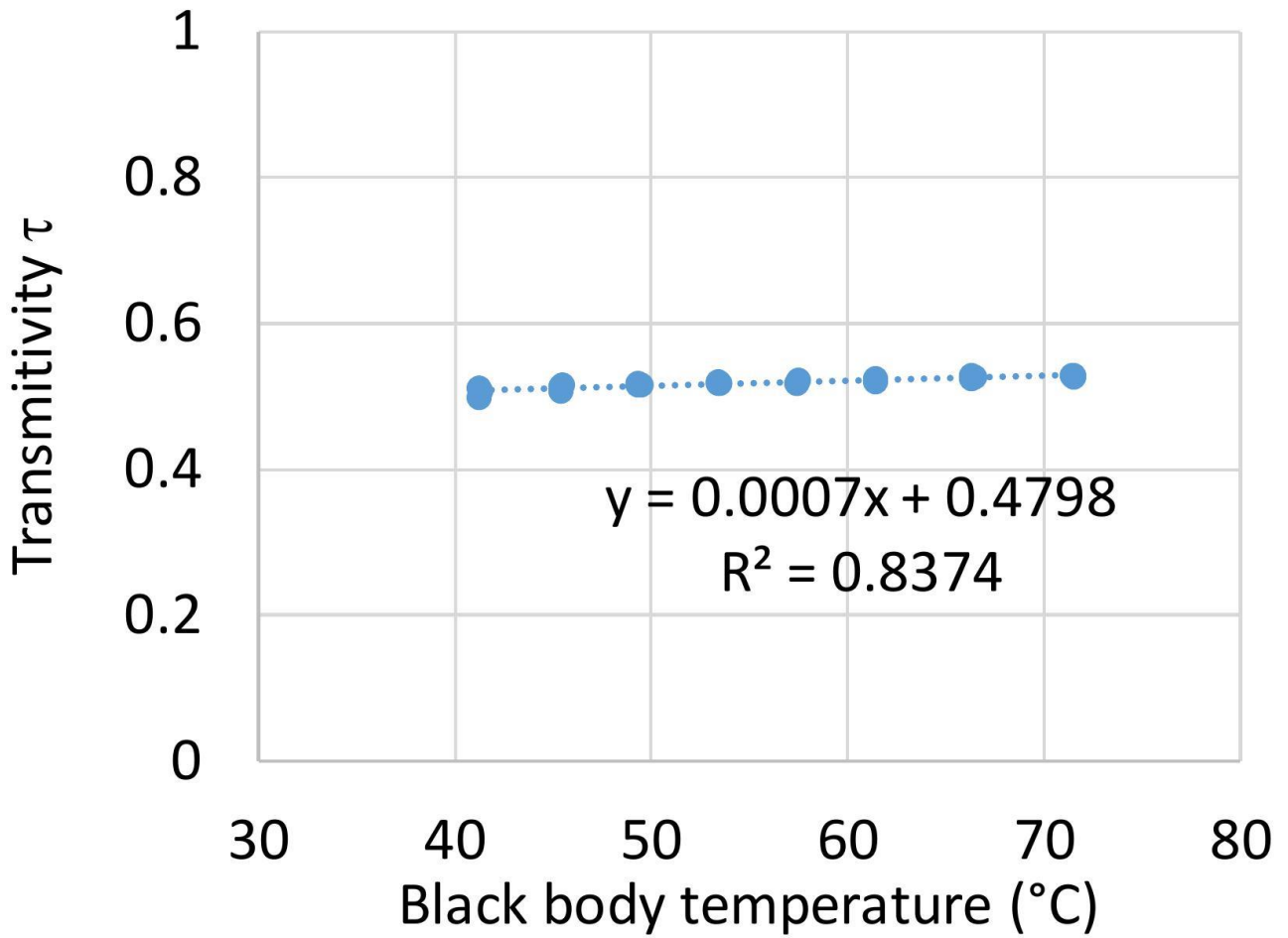
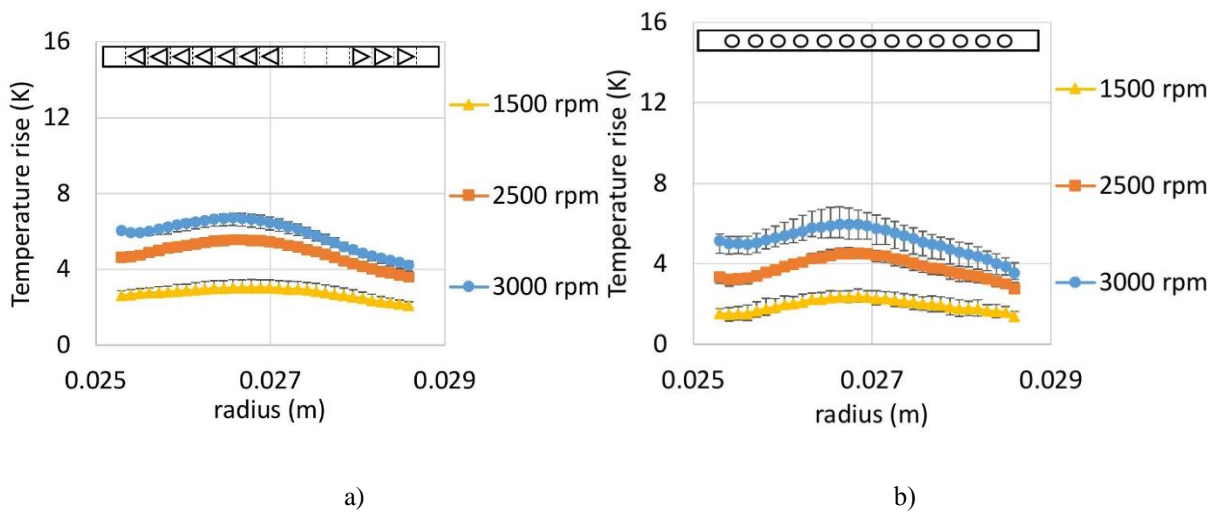


Fig. 8 Transmissivity of the sapphire as a function of the black body temperature



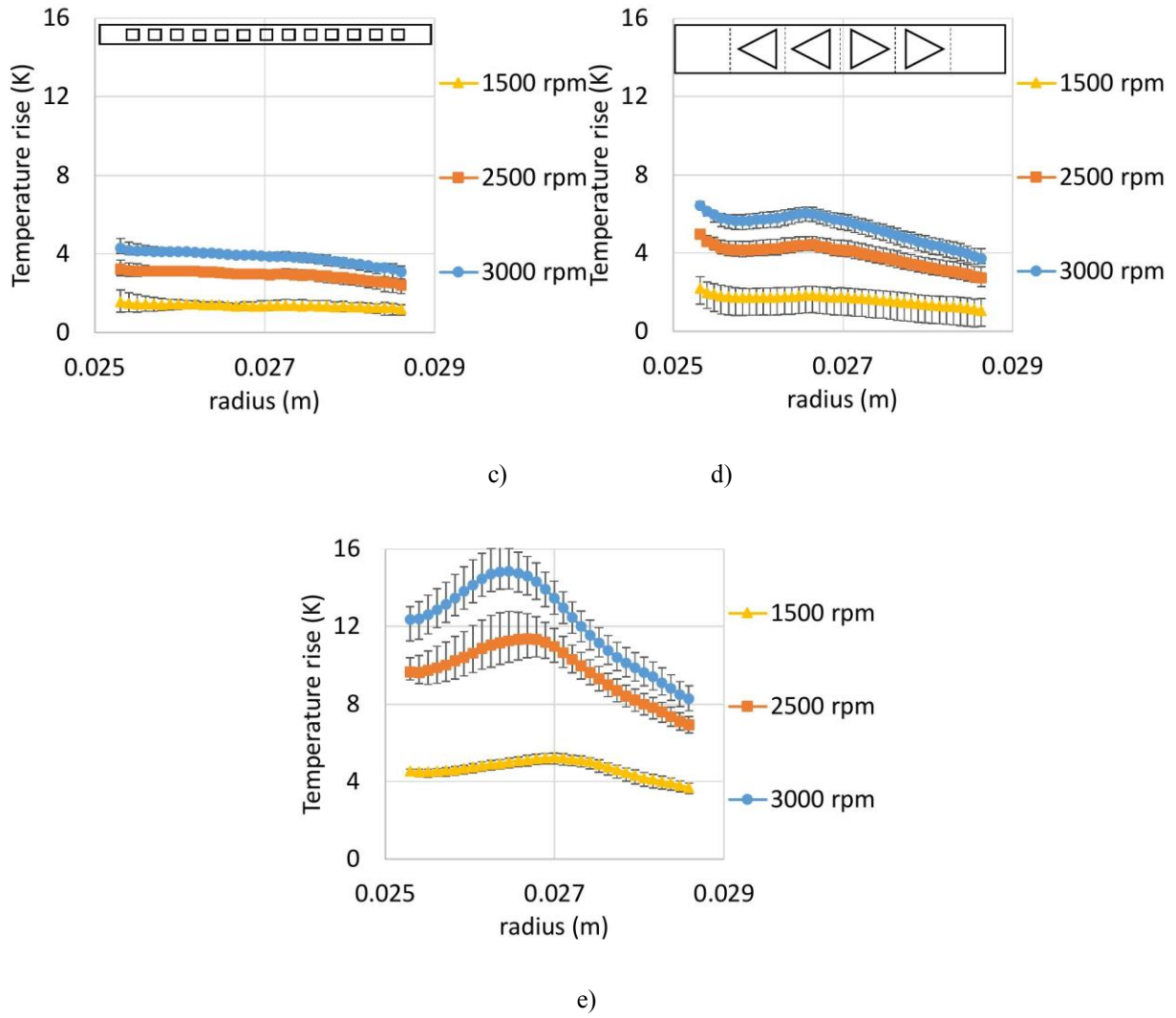


Fig. 9 Radial temperature profiles at different operating speeds: a) triangle 1 -b) circle – c) square – d) triangle 2 – e) smooth.

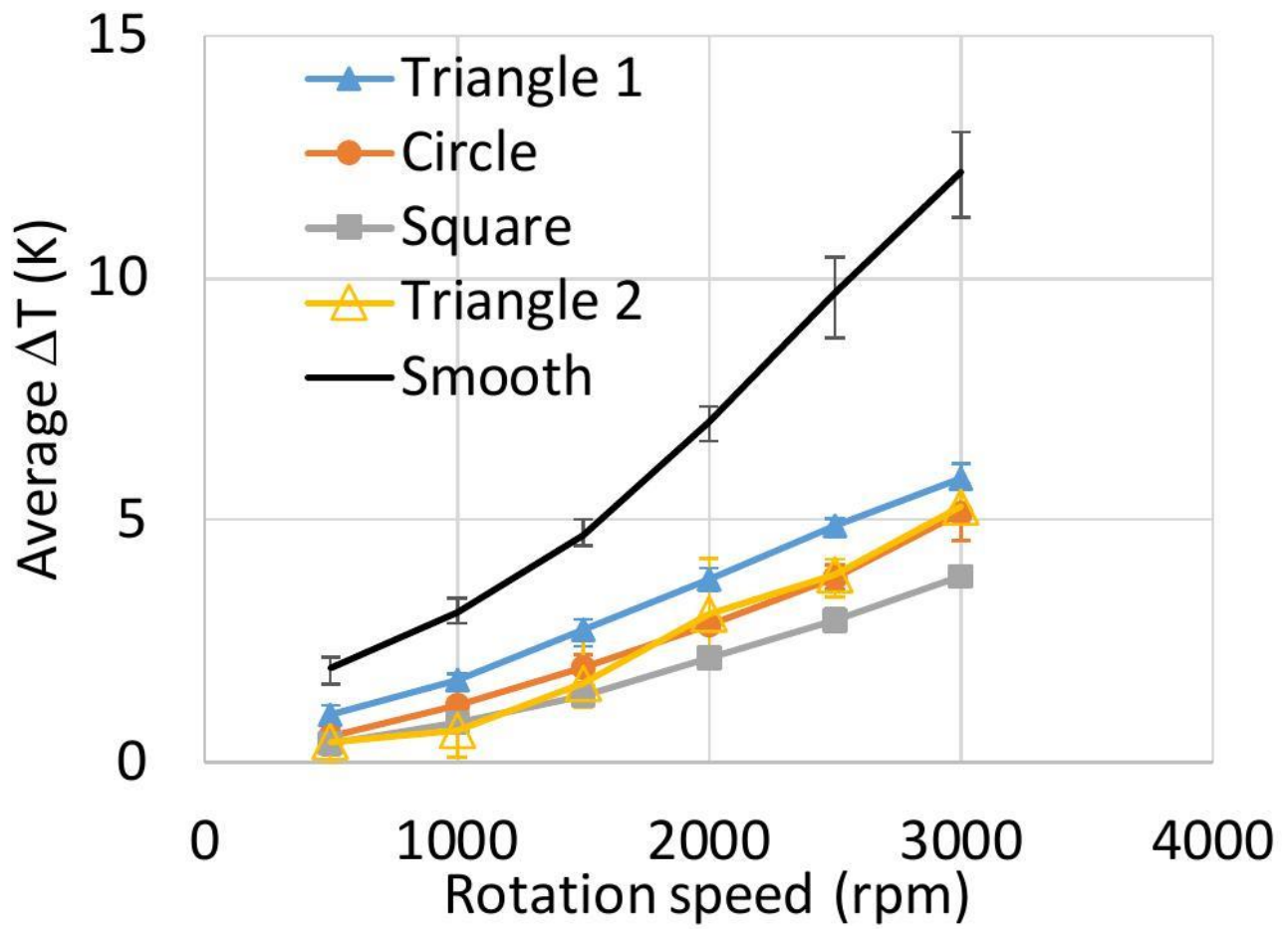


Fig. 10 Average temperature rise in the contact as a function of speed for the different surfaces.

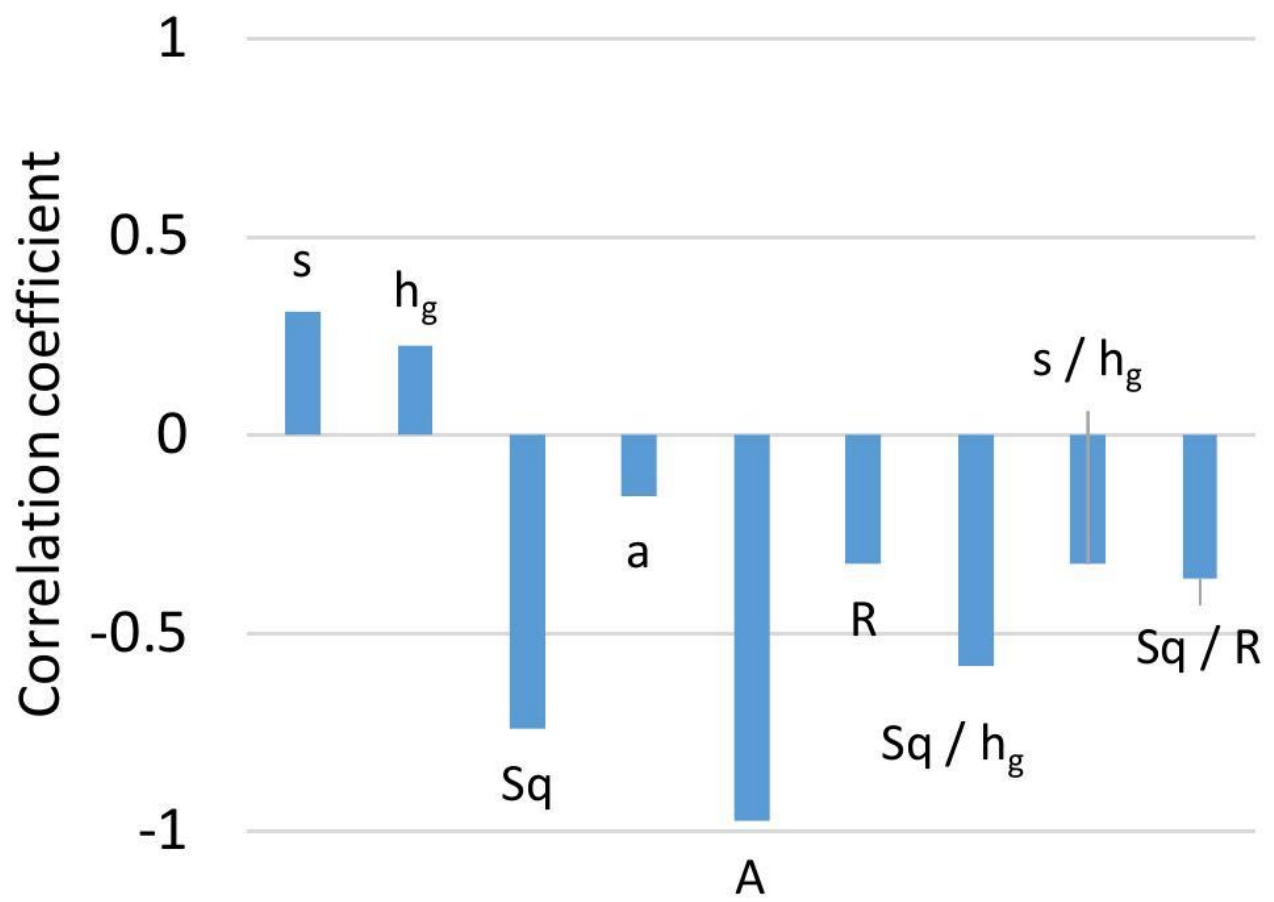


Fig. 11 Correlation between the texture parameters and the temperature rise

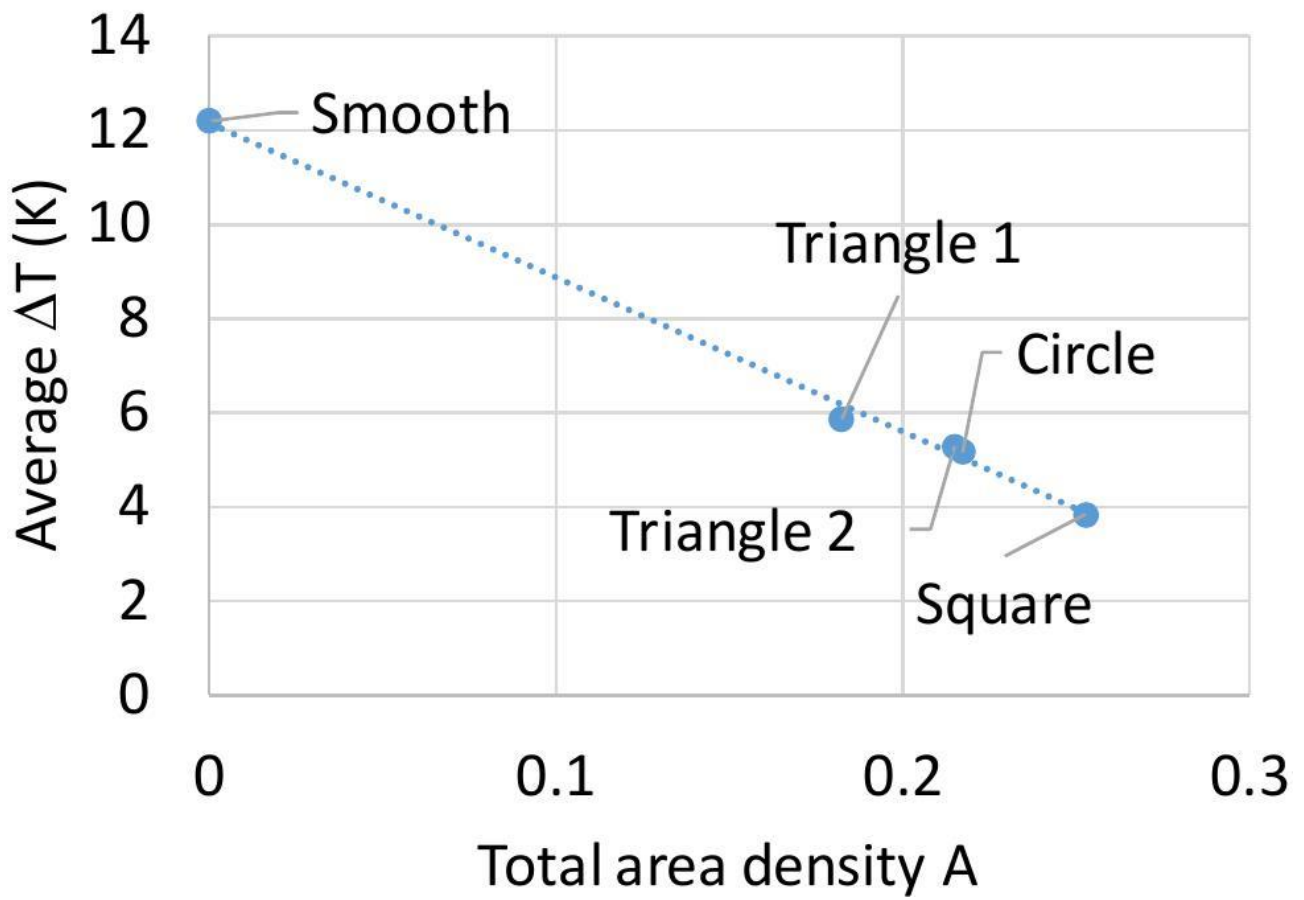


Fig. 12 Temperature rise at 3000 rpm as a function of the geometrical parameter T (3)

Table 1 Mechanical seal characteristics

Parameter	Value
Outer radius R_o (mm)	28.8
Inner radius R_i (mm)	25.8
Closing force (at 0.5 MPa)	316.6 N

Table 2 Seal surface characteristics

Surface pattern	Groove size s (μm)	Groove depth h_g (μm)	Roughness Sq (μm)
Triangle 1	159	0.25	0.087
Circle	113	0.31	0.076
Square	108	0.23	0.116
Triangle 2	431.5	0.22	0.10
Smooth			0.12

Table 3 Operating conditions

Parameter	Value
Outer pressure (MPa)	0.5
Inner pressure (MPa)	0
Fluid	Water
Fluid temperature	40°C
Rotating speed (rpm)	500 - 3000
Test duration per condition (min)	~ 10

Table 4 Refraction indices of the media

Medium	Refractive index n
Air	1.00029
Water	1.333
Sapphire	1.75

Table 5 Texture geometrical parameters

Parameter	Triangle 1	Circle	Square	Triangle 2
Groove size s (μm)	159	113	108	431.5
Groove depth h_g (μm)	0.25	0.31	0.23	0.22
Surface roughness Sq	0.087	0.076	0.116	0.1

(μm)				
Surface radius of curvature R (m)	0.63	0.56	0.80	0.93
Local area density a	0.274	0.251	0.292	0.322
Total area density A	0.1822	0.217	0.25272	0.215
Sq / h_g	0.348	0.245	0.5046	0.454
Aspect ratio h_g / s	0.00157	0.00274	0.00212	0.000509
Surface defect ratio Sq / R (10^{-7})	1.38	1.36	1.44	1.07
Temp. rise ΔT (K) at 3000 rpm	5.86	5.15	3.84	5.28